

# Fast method for inverse determination of optical parameters from two measured signals

Xun Chen,<sup>1</sup> Yuanming Feng,<sup>1,2</sup> Jun Q. Lu,<sup>2</sup> Xiaohui Liang,<sup>3</sup> Jue Ding,<sup>3</sup> Yong Du,<sup>4</sup> and Xin-Hua Hu<sup>2,1,\*</sup>

<sup>1</sup>Department of Biomedical Engineering, Tianjin University, Tianjin 300072, China

<sup>2</sup>Department of Physics, East Carolina University, Greenville, North Carolina 27858, USA

<sup>3</sup>Experimental Instrument Plant, AMMS, Beijing 100850, China

<sup>4</sup>Department of Radiology, The John Hopkins University, Baltimore, Maryland 21287, USA

\*Corresponding author: hux@ecu.edu

Received March 15, 2013; revised April 21, 2013; accepted May 20, 2013;  
posted May 20, 2013 (Doc. ID 187100); published June 10, 2013

Solving inverse problems requires multiple forward calculations of measured signals. We present a fast method combining graphic processing unit-accelerated Monte Carlo simulations of individual photons and a new perturbation scheme for a 300-fold speedup in comparison to conventional CPU-based approaches. The method allows rapid calculations of the diffuse reflectance and transmittance signals from a turbid sample of absorption coefficient  $\mu_a$ , scattering coefficient  $\mu_s$ , and anisotropy factor  $g$  based on the principle of correlated sampling. To demonstrate its strong utility, we have applied the method for determining the optical parameters of diluted intralipid samples with satisfactory results. © 2013 Optical Society of America

OCIS codes: (290.3200) Inverse scattering; (120.5820) Scattering measurements.

<http://dx.doi.org/10.1364/OL.38.002095>

It remains a challenging problem to accurately and rapidly determine the absorption coefficient  $\mu_a$ , scattering coefficient  $\mu_s$ , and anisotropy factor  $g$  of a turbid sample from the measured signals. Solving such an inverse problem iteratively requires forward solutions of a boundary-value problem defined by the radiative transfer equation and Fresnel equations [1,2]. We have previously used an integrating sphere to measure diffuse reflectance  $R_d$  and transmittance  $T_d$ . A Monte Carlo (MC) method was employed as the forward boundary-value problem solver to inversely determine  $\mu_s$  and  $g$  from  $R_d$  and  $T_d$  after obtaining the attenuation coefficient  $\mu_t (= \mu_a + \mu_s)$  from the forward transmittance signals [2,3].

Despite their accuracy, MC methods are computationally expensive and especially so for solving inverse problems requiring multiple iterations [4]. With an integrating sphere one can drastically reduce the time of MC simulations of  $R_d$  and  $T_d$  because they are acquired as hemispherically averaged signals over a solid angle close to  $2\pi$  (sr). For example, only  $7 \times 10^5$  photons need to be tracked in one MC simulation to keep the fluctuation of the simulated signals less than 2%, which can be completed in about 1 min on a regular personal computer [3]. The use of an integrating sphere, however, presents a considerable constraint on implementation because it increases preparation time, cost, and size of the instrument. In this Letter, we present a fast method that can significantly reduce the computational cost of tracking  $10^8$  or more photons. With this method, only two single detectors suffice to measure  $R_d$  and  $T_d$ .

Figure 1 shows the considered configuration of a turbid sample confined in a holder and two detectors to collect photons injected at an incident angle of  $\theta_0$  and scattered by the sample. The two detectors are placed in the horizontal ( $x$ - $z$ ) plane with sensor surfaces facing the sample with  $d_R$  and  $d_T$  as the distances to the center of holder surfaces and  $\theta_R$  and  $\theta_T$  as the orientation angles. In this case each detector is assumed to have a

round sensor area of 4 mm diameter, and the efficiencies of photon detection are very low with solid angles of about  $3.5 \times 10^{-3}$  (sr) for  $d_R = d_T = 60$  mm. Clearly a fast method to rapidly calculate  $R_d$  and  $T_d$  is highly desired for inverse determination of  $\mu_s$  and  $g$ .

The new method is based on an MC algorithm of tracking individual photons (iMC) developed in our group with numerous validations [2,5–8]. Different from the conventional one [4,9,10], the iMC algorithm interprets light absorption as the termination of tracked photons instead of distribution along a trajectory. Tracking individual photons allows the iMC algorithm to treat complex boundary conditions, such as diverging or converging incident beams and samples with rough surfaces [7,11]. Briefly, iMC starts by obtaining a total travel distance  $L_a$  from  $\mu_a$  and a random number (RND) uniformly distributed in  $[0,1]$  as given in Eq. (1) before a photon is launched according to the Fresnel equations at the sample surface. After launching, the photon undergoes a random-walk process with a sequence of travel distances ( $L_{sj}$ ;  $i = 1, 2, \dots, k$ ) determined by  $\mu_s$  and directions by  $g$ , assuming the Henyey–Greenstein function as the scattering phase function. At the end of each segment  $L_{sj}$ , the fate of photon is determined by comparing the accumulated path length  $L_s$  to  $L_a$ , where

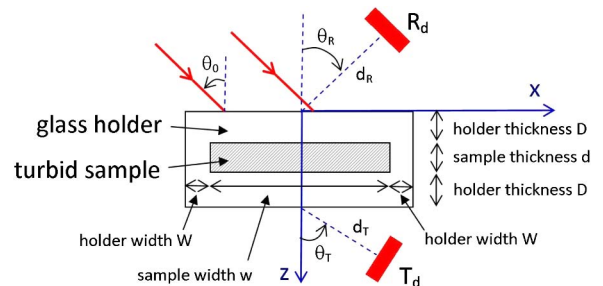


Fig. 1. Schematic of the source-sample-detector configuration (not to scale) with beam center at  $(x_0, 0, 0)$ , diameter  $B$ , and a top-hat beam profile.

$$L_a = \frac{-\ln(\text{RND})}{\mu_a}, \quad L_{si} = \frac{-\ln(\text{RND})}{\mu_s} \quad \text{and} \quad L_s = \sum_{i=1}^j L_{si}. \quad (1)$$

If  $L_s > L_a$ , the photon is terminated as being absorbed; otherwise it is propagated further. Once a photon reaches the sample boundary, its incident angle and the mismatched refractive indices decide whether the photon returns or exits into the surrounding nonscattering media according to the Fresnel equations. For exiting photons, those eventually reaching a detector are registered as the calculated signals of  $R_d$  or  $T_d$  after normalization by the number of incident photons.

The new method consists of two improvements of efficiency. The first converts the iMC code from central processing unit (CPU) into graphic processing unit (GPU) execution to take advantage of parallel computing by multiple GPUs based on a code design published in [12]. In GPU-iMC simulations, different seeds for obtaining RND sequences are used in different GPUs, which are provided by the CPU executed portion of the code to ensure independent sampling. The average speedup for the iMC simulations executed on a low-cost graphic board (NVIDIA GT640) is about 20 in comparison to simulations run on an Intel dual-core CPU of 3.2 GHz. The speedup could be further improved if another graphic board is used for display. To track  $2.0 \times 10^8$  photons for configurations similar to those in Fig. 2, it takes from 3 to 6 min to complete with fluctuations of the estimated  $R_d$  or  $T_d$  values kept at 0.5% or less.

For the second improvement, we developed a new scheme to calculate  $R_d$  or  $T_d$  for a “perturbed” sample of  $\mu_a$ ,  $\mu_s$  and  $g$  from an “unperturbed” or reference sample of  $\mu_{a0} = 0$ ,  $\mu_{s0}$ , and  $g_0$ . The new scheme follows the same assumption made by the previous method [9,13,14] that two samples sufficiently similar to each other share the same set of photons contributing to the signals. To arrive at a procedure applicable to the iMC algorithm, we have investigated the dependence of  $R_d$  and  $T_d$  on  $\mu_a$ ,  $\mu_s$  and  $g$  in various configurations. In the case of  $\mu_a$ , the two samples are very similar because absorption merely reduces the number of registered photons for the perturbed sample from the reference one without modifying their trajectories. For scattering parameters, trajectories are varied, and the ranges of  $\mu_s$  and  $g$  from their reference values have to be limited to keep sufficient similarity.

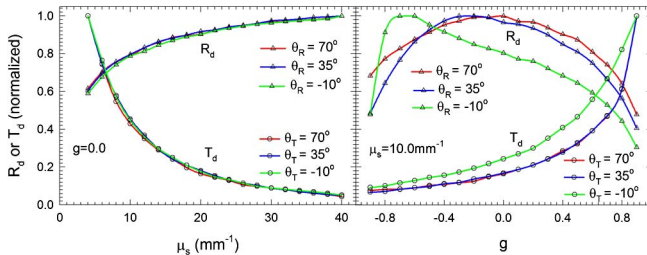


Fig. 2.  $R_d$  and  $T_d$  versus  $\mu_s$  and  $g$  with  $\mu_a = 0.1 \text{ mm}^{-1}$ ,  $d_R = d_T = 60 \text{ mm}$ ,  $x_0 = 0 \text{ mm}$ ,  $B = 6.35 \text{ mm}$ ,  $\theta_0 = 45^\circ$ ;  $d = 1 \text{ mm}$ ,  $w = 25 \text{ mm}$ , sample height along the  $y$  axis is  $25 \text{ mm}$ ,  $W = 1 \text{ mm}$ ,  $D = 3 \text{ mm}$ , refractive index  $n = 1.349$  for the sample, and  $n' = 1.519$  for the holder. Symbols are simulation results, and solid curves are guides for the eye.

Figure 2 presents typical examples of these relations. Similar results were obtained for other source–detector configurations. These data show that variation of  $g$  leads to fairly complex change patterns in the  $R_d$  signal. Rule (ii) below has been devised to calculate  $R_d$  and  $T_d$  from  $\mu_s$  and  $g$  varied from a reference sample according to the relations in Fig. 2. For example, as  $\mu_s$  increases from  $\mu_{s0}$  or positive  $\Delta\mu_s$ ,  $R_d$  increases while  $T_d$  decreases, which yields the definitions of  $m$  and  $m'$  in Eqs. (2) and (3).

At the beginning a full GPU-iMC simulation is performed to store  $L_{s0}$  for each registered photon of  $R_d$  or  $T_d$  for the reference sample. Note that  $\mu_{a0} = 0$ , and consequently no photon is absorbed in the reference sample. Then the stored data are retrieved to examine whether each registered photon still contributes to the  $R_d$  or  $T_d$  signals for a perturbed sample according to the two rules below:

(i) With  $\mu_a$  updated from  $\mu_{a0} = 0$  to a finite value, a finite  $L_a$  can now be obtained from Eq. (1). If the accumulated path length of a registered photon  $L_{s0} \geq L_a$ , it is eliminated from the detected signals for the perturbed sample. Otherwise one proceeds to the next rule to determine whether the photon still can be detected.

(ii) For  $g_0 > 0$ , the accumulated path length  $L_s$  is obtained from  $L_{s0}$  according to

$$L_s = \left[ 1 + (-1)^m \frac{\Delta\mu_s}{\mu_{s0}} + (-1)^{m'} \frac{\Delta g}{1 - g_0} \right]^{-1} L_{s0}, \quad (2)$$

where  $\Delta\mu_s = \mu_s - \mu_{s0}$ ,  $\Delta g = g - g_0$ ,  $m$  and  $m' = 0$  or  $1$ . For the  $R_d$  signal  $m = 0$  and  $m' = 1$ , while for  $T_d$   $m = 1$  and  $m' = 0$ . If  $g_0 \leq 0$ , Eq. (2) is replaced by

$$L_s = \left[ 1 + (-1)^m \frac{\Delta\mu_s}{\mu_{s0}} + (-1)^{m'} \Delta g \right]^{-1} L_{s0}, \quad (3)$$

where the value of  $m$  remains the same as before and  $m' = 0$  for the  $T_d$  signal. For the  $R_d$  signal,  $m'$  becomes source–detector dependent, with  $m' = 1$  for  $|g| \leq \cos(\theta_0 + \theta_R)$  and  $m' = 0$  otherwise. After  $L_s$  is updated for each registered photon that passes rule (i), those of  $L_s \geq L_a$  are eliminated.

After elimination, the survival photons will be registered for  $R_d$  and  $T_d$ , respectively, for the perturbed sample. To examine the accuracy, we have compared the signals obtained by the new scheme to those calculated by the full GPU-iMC simulations for the same sets of reference and perturbed samples. Two examples of the relative differences are shown in Figs. 3 and 4, each of which was calculated on 49 sets of  $\mu_s$  and  $g$  with fixed  $\mu_a$ . The relative changes of  $\mu_s$  and  $g$  for the perturbed sample were kept within  $\pm 10\%$  of those of the reference sample.

From the above results one can see that the new scheme allows rapid calculations of  $R_d$  and  $T_d$  with both  $\mu_s$  and  $g$  perturbed from the reference sample and  $\mu_a$  set to arbitrary values from  $\mu_{a0} = 0$ . The calculated signals exhibit quite different sensitivities to the change of  $\mu_s$  and  $g$  with errors of  $R_d$  less than  $\pm 4\%$  and those of  $T_d$  less than  $\pm 6\%$ . These errors are tolerable in inverse determination of the optical parameters, since they are

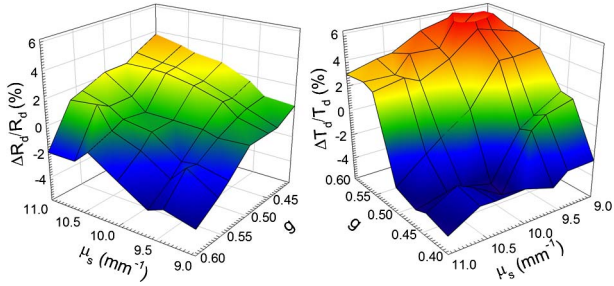


Fig. 3. Dependence of  $\Delta R_d/R_d$  and  $\Delta T_d/T_d$  on  $\mu_s$  and  $g$  with  $\mu_a = 0.05 \text{ mm}^{-1}$ ,  $\mu_{s0} = 10.0 \text{ mm}^{-1}$ ,  $g_0 = 0.5$ , and  $\theta_R = \theta_T = 70^\circ$ ; all other parameters are the same as those in Fig. 2.

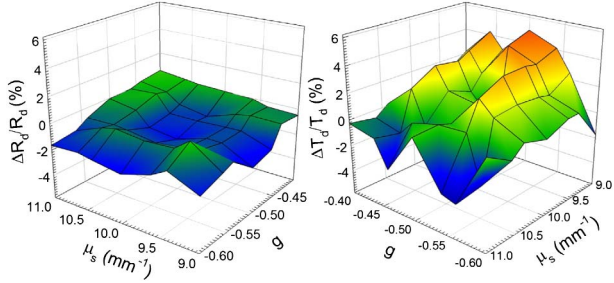


Fig. 4. Dependence of  $\Delta R_d/R_d$  and  $\Delta T_d/T_d$  on  $\mu_s$  and  $g$  with  $\mu_a = 0.1 \text{ mm}^{-1}$ ,  $\mu_{s0} = 10.0 \text{ mm}^{-1}$ ,  $g_0 = -0.5$ , and  $\theta_R = \theta_T = 70^\circ$ ; all other parameters are the same as those in Fig. 2.

often less or much less than the errors of measured signals.

To demonstrate the utility of the fast method we have applied it to the determination of  $\mu_s$  and  $g$  from the measured signals of  $R_d$  and  $T_d$  from 0.8% intralipid solution samples diluted from 30% intralipid with distilled water as functions of wavelength from 510 to 690 nm. The measurements were performed in a configuration similar to Fig. 1 with the forward transmittance  $T_f$  acquired at three values of sample thickness  $d = 1, 2, \text{ and } 3 \text{ mm}$ . From the  $T_f$  versus  $d$  data,  $\mu_t$  was determined by using the Beer-Lambert law [3]. Afterward  $\mu_s$  and  $g$  were determined using a gradient based algorithm [3] to search for optimized values so that the calculated  $R_d$  and  $T_d$  matched the measured values within 5% for the sample of different  $d$ ,  $\theta_0 = 7^\circ$ ,  $d_R = 63 \text{ mm}$ ,  $\theta_R = 29^\circ$ ,  $d_T = 82 \text{ mm}$ , and  $\theta_T = -27^\circ$ . The results shown in Fig. 5 are consistent with our previous ones, while the values of  $\mu_a$  are higher than those obtained by other groups, possibly due to the existence of a detection floor [3]. The relative difference of the inversely determined parameters between the new method and full MC simulations are mostly negligible except in the cases of longer wavelengths, where  $\mu_a$  is very small and errors of inverse solutions are large. The total time for obtaining the parameters at the 10 wavelengths was 7.35 min to run 3 full GPU-iMC simulations of  $1.1 \times 10^8$  photons and 112 min without the perturbation method, which took 57 full simulations. Together, a 300-fold speedup was

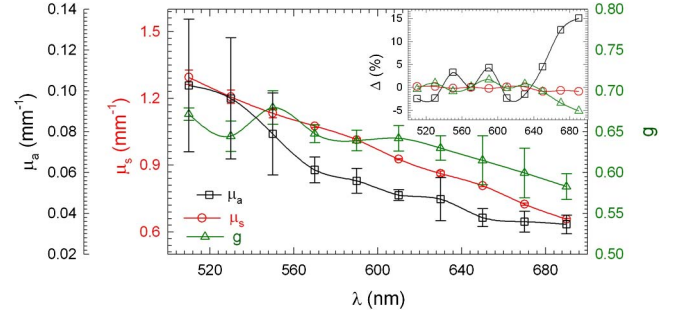


Fig. 5. Wavelength dependence of optical parameters inversely determined from three samples of  $d = 1, 2, 3 \text{ mm}$  with symbols representing the mean values and error bars the standard deviations. Inset, the relative difference  $\Delta$  between the parameters determined by the new method and those with full GPU-iMC simulations for the sample with  $d = 2 \text{ mm}$ . The solid curves are guides for the eye.

achieved in comparison to the conventional CPU-based approaches [2,3].

In summary, we have developed a fast perturbation method for GPU-MC simulations to inversely determine optical parameters from measured signals. The new method requires minimal data storage and communication, which is particularly advantageous for GPU execution over the previous methods [13,14]. Much improved efficiency is expected for the fast method if multiple sets of the  $\mu_a$ ,  $\mu_s$ , and  $g$  parameters are to be determined from, for example, the reflectance image data from a heterogeneous turbid sample [8].

Y. Feng acknowledges support by the NSFC (grants 81171342 and 81201148).

## References

1. S. A. Prahl, M. J. C. van Gemert, and A. J. Welch, *Appl. Opt.* **32**, 559 (1993).
2. Y. Du, X. H. Hu, M. Cariveau, X. Ma, G. W. Kalmus, and J. Q. Lu, *Phys. Med. Biol.* **46**, 167 (2001).
3. C. Chen, J. Q. Lu, H. Ding, K. M. Jacobs, Y. Du, and X. H. Hu, *Opt. Express* **14**, 7420 (2006).
4. J. Spanier and E. M. Gelbard, *Monte Carlo Principles and Neutron Transport Problems* (Addison-Wesley, 1969).
5. Z. Song, K. Dong, X. H. Hu, and J. Q. Lu, *Appl. Opt.* **38**, 2944 (1999).
6. X. Ma, J. Q. Lu, R. S. Brock, K. M. Jacobs, P. Yang, and X. H. Hu, *Phys. Med. Biol.* **48**, 4165 (2003).
7. X. Ma, J. Q. Lu, H. Ding, and X. H. Hu, *Opt. Lett.* **30**, 412 (2005).
8. C. Chen, J. Q. Lu, K. Li, S. Zhao, R. S. Brock, and X. H. Hu, *Med. Phys.* **34**, 2939 (2007).
9. H. Rief, *Ann. Nucl. Energy* **11**, 455 (1984).
10. L. Wang, S. L. Jacques, and L. Zheng, *Comput. Meth. Prog. Bio.* **47**, 131 (1995).
11. X. Ma, J. Q. Lu, and X. H. Hu, *Opt. Lett.* **28**, 2204 (2003).
12. E. Alerstam, W. C. Yip Lo, T. D. Han, J. Rose, S. Andersson-Engels, and L. Lilje, *Biomed. Opt. Express* **1**, 658 (2010).
13. C. K. Hayakawa, J. Spanier, F. Bevilacqua, A. K. Dunn, J. S. You, B. J. Tromberg, and V. Venugopalan, *Opt. Lett.* **26**, 1335 (2001).
14. A. Sassaroli, *Opt. Lett.* **36**, 2095 (2011).